



2D Materials Hot Paper

How to cite: *Angew. Chem. Int. Ed.* **2020**, 59, 23620–23625

International Edition: doi.org/10.1002/anie.202010398

German Edition: doi.org/10.1002/ange.202010398

Synthesis of Vinylene-Linked Two-Dimensional Conjugated Polymers via the Horner–Wadsworth–Emmons Reaction

Dominik L. Pastoetter, Shunqi Xu, Mino Borrelli, Matthew Addicoat, Bishnu P. Biswal, Silvia Paasch, Arezoo Dianat, Heidi Thomas, Reinhard Berger, Sebastian Reineke, Eike Brunner, Gianauelio Cuniberti, Marcus Richter, and Xinliang Feng*

Abstract: In this work, we demonstrate the first synthesis of vinylene-linked 2D CPs, namely, 2D poly(phenylenequinoxalinevinylene)s **2D-PPQV1** and **2D-PPQV2**, via the Horner–Wadsworth–Emmons (HWE) reaction of C_2 -symmetric 1,4-bis(diethylphosphonomethyl)benzene or 4,4'-bis(diethylphosphonomethyl)biphenyl with C_3 -symmetric 2,3,8,9,14,15-hexa(4-formylphenyl)diquinoxalino[2,3-a:2',3'-c]phenazine as monomers. Density functional theory (DFT) simulations unveil the crucial role of the initial reversible C–C single bond formation for the synthesis of crystalline 2D CPs. Powder X-ray diffraction (PXRD) studies and nitrogen adsorption-desorption measurements demonstrate the formation of proclaimed crystalline, dual-pore structures with surface areas of up to $440\text{ m}^2\text{ g}^{-1}$. More importantly, the optoelectronic properties of the obtained **2D-PPQV1** ($E_g = 2.2\text{ eV}$) and **2D-PPQV2** ($E_g = 2.2\text{ eV}$) are compared with those of cyano-vinylene-linked **2D-CN-PPQV1** ($E_g = 2.4\text{ eV}$) produced by the Knoevenagel reaction and imine-linked 2D COF analog (**2D-C=N-PPQV1**, $E_g = 2.3\text{ eV}$), unambiguously proving the superior conjugation of the vinylene-linked 2D CPs using the HWE reaction.

The exploration of poly(acetylene) in 1977 by SHIRAKAWA et al.^[1] has led to the development of various linear conjugated polymers, which have been widely used in applications such as organic field-effect transistors (OFETs),^[2] organic light-emitting diodes (OLEDs),^[2,3] energy storage^[4] and conversion,^[2,3] optical sensing,^[5] biomedical applications,^[6] and lasers.^[7] In contrast to investigations of linear conjugated polymers and their applications, the successive

increase in dimension caused by covalently connecting multiple strands to form two-dimensional conjugated polymers (2D CPs) remains mostly unexplored. Graphene is a prototype 2D conjugated polymer consisting of multiple strands of poly-*p*-phenylene that are interconnected, leading to a hexagonal network of sp^2 -hybridized carbon atoms.^[8] Graphene is semimetallic in nature with zero band gap and high charge carrier mobility.^[9] Therefore, structurally defined 2D CPs with π -electron delocalization in two dimensions are expected to offer highly desirable properties for organic optoelectronics, such as an ideal band structure for superior charge carrier mobility, tailorable highest occupied molecular orbital-lowest unoccupied molecular orbital (HOMO–LUMO) band gaps, and defect tolerance enabled by increased dimensionality in comparison to that of linear conjugated polymers.^[10]

In contrast to the emergent 2D π -conjugated covalent organic frameworks (COFs), which can be regarded as 2D CPs and have thus far been dominated by Schiff base reactions,^[11] the synthesis of 2D CPs with fully sp^2 -carbon-linked backbones still lacks effective protocols to generate crystalline polymer materials.^[12] In particular, sp^2 -carbon-linked (or vinylene-linked) 2D CPs provide high chemical and thermal stabilities as well as complete π -conjugation over the whole 2D polymer framework, making these materials highly attractive for various applications, such as in optoelectronics, spintronics, and energy storage.^[13–15] Thus far, only Knoevenagel^[13–15,16] and other aldol-type condensation^[17–19] reactions have been reported for the synthesis of crystalline vinylene-linked 2D CPs. However, Knoevenagel polycondensation provides cyano-vinylene-linked 2D CPs in which additional

[*] M. Sc. D. L. Pastoetter, M. Sc. S. Xu, M. Sc. M. Borrelli, Dr. R. Berger, Dr. M. Richter, Prof. Dr. X. Feng
Chair of Molecular Functional Materials, Center for Advancing Electronics Dresden (cfaed) and Faculty of Chemistry and Food Chemistry, Technische Universität Dresden
01062 Dresden (Germany)
E-mail: xinliang.feng@tu-dresden.de

Dr. M. Addicoat
School of Science and Technology, Nottingham Trent University
Nottingham, NG118NS (UK)

Dr. B. P. Biswal
Department of Chemistry, Ashoka University
Rajiv Gandhi Education City, Sonapat (Delhi NCR), Haryana 131029 (India)

Dr. S. Paasch, Prof. Dr. E. Brunner
Chair of Bioanalytical Chemistry, Faculty of Chemistry and Food Chemistry, Technische Universität Dresden
01062 Dresden (Germany)

Dr. A. Dianat, Prof. Dr. G. Cuniberti
Chair of Material Science and Nanotechnology, Faculty of Mechanical Science and Engineering, Technische Universität Dresden
01062 Dresden (Germany)

Dr. H. Thomas, Prof. Dr. S. Reineke
Dresden Integrated Center for Applied Physics and Photonic Materials (IAPP), Technische Universität Dresden
01187 Dresden (Germany)

Supporting information and the ORCID identification number(s) for the author(s) of this article can be found under:
<https://doi.org/10.1002/anie.202010398>.

© 2020 The Authors. Angewandte Chemie International Edition published by Wiley-VCH GmbH. This is an open access article under the terms of the Creative Commons Attribution Non-Commercial NoDerivs License, which permits use and distribution in any medium, provided the original work is properly cited, the use is non-commercial and no modifications or adaptations are made.

cyano-groups on the conjugated backbone cause structural twisting due to steric hindrance.^[20] In contrast, the reported synthesis of unsubstituted vinylene-linked 2D CPs *via* other aldol-type polycondensations has been limited to electron-deficient mesitylene building blocks, such as 2,4,6-trimethyl-1,3,5-triazine (TMT) and 3,5-dicyano-2,4,6-trimethylpyridine (DCTMP).^[17,18] Therefore, the synthesis of vinylene-linked 2D CPs with tailorable properties employing robust monomer combinations requires rapid development of novel synthetic protocols. The Horner–Wadsworth–Emmons (HWE) reaction is a chemical reaction between phosphonates and aldehydes to produce predominantly *trans*-vinylenes.^[21] It offers stabilized ylide carbanions and therefore reversibility of the initial C–C single bond formation.^[22,23] Due to the lower activation energy of the irreversible step for the *trans*-vinylene, the HWE reaction is not only thermodynamically but also kinetically controlled, favoring the formation of *trans*-vinylenes.^[23]

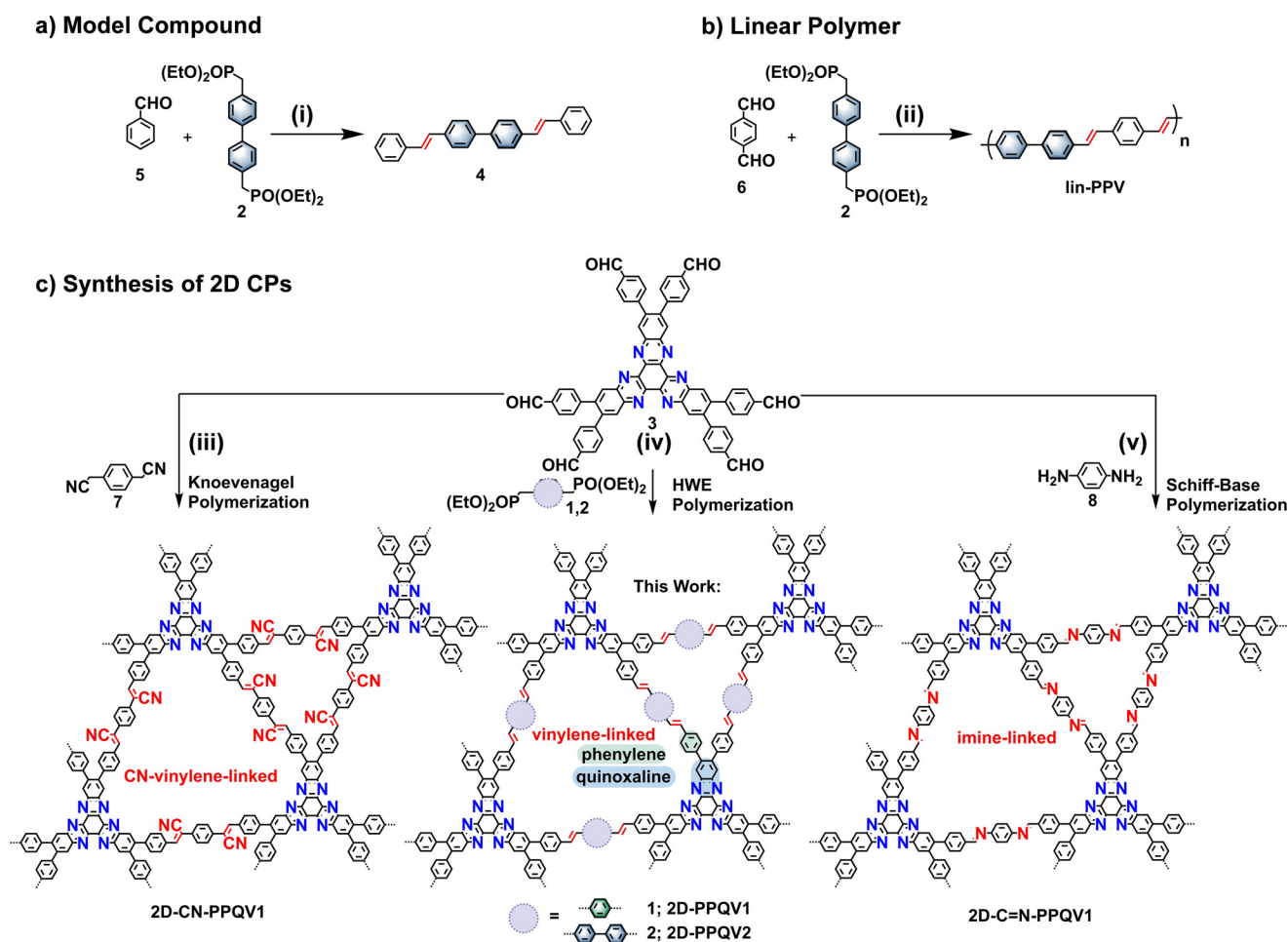
In this work, we demonstrate the first synthesis of quinoxaline-incorporated two-dimensional poly(arylenevinylene)s, namely, 2D-poly(phenylenequinoxalinevinylene)s **2D-PPQV1** and **2D-PPQV2**, by employing the HWE reaction of 1,4-bis(diethylphosphonomethyl)benzene (**1**) or 4,4'-bis(diethylphosphonomethyl)biphenyl (**2**) with 2,3,8,9,14,15-hexa(4-formylphenyl)diquinoxalino[2,3-*a*:2',3'-*c*]phenazine (HATN-6CHO, **3**). Density functional theory (DFT) simulations unveil the crucial role of the initial reversible C–C single bond formation in the synthesis of crystalline 2D-PPQVs. The vinylene-linked dual-pore structures of **2D-PPQV1** and **2D-PPQV2** are disclosed by nitrogen physisorption measurements, showing two main pore size distributions and surface areas of up to 440 m² g⁻¹. Remarkably, a comparison of the optoelectronic properties of **2D-PPQV1** ($E_g = 2.2$ eV) and **2D-PPQV2** ($E_g = 2.2$ eV) with those of cyano-vinylene-linked **2D-CN-PPQV1** ($E_g = 2.4$ eV) and imine-linked 2D COF analog unambiguously demonstrates the narrower energy gap and superior conjugation of the 2D CPs synthesized by HWE polymerization.

To explore and understand the HWE reaction, different model reactions were first employed: We synthesized the A₁B₂-type model compound 4,4'-di(*E*-styryl)-1,1'-biphenyl (**4**) from benzaldehyde (**5**) and 4,4'-bis(diethyl-phosphonomethyl)biphenyl (**2**) with Cs₂CO₃ as the base, with an isolated yield of 80% (Scheme 1a). Model compound **4** was fully characterized by nuclear magnetic resonance (NMR) spectroscopy and high-resolution matrix-assisted laser desorption/ionization time-of-flight mass spectrometry (HR-MALDI-TOF-MS) (see the Supporting Information). Under the same reaction conditions, an A₂B₂-type linear poly(*p*-phenylene vinylene) (**lin-PPV**) based on terephthalaldehyde (**6**) and 4,4'-bis(diethyl-phosphonomethyl)biphenyl (**2**) was synthesized in a yield of 79% (Scheme 1b). Due to the low solubility of the unsubstituted **lin-PPV**, precipitation of the polymer occurred within hours. ¹³C-ssNMR and FTIR spectroscopy manifested the successful formation of the linear polymer (see Supporting Information). Moreover, the MALDI-TOF-MS spectrum demonstrated a molecular weight of up to 8800 gmol⁻¹ (corresponding to 31 repeat

units), which suggested an efficient polymerization degree (see the Supporting Information).

Motivated by the efficiency of the model reactions and the linear polymerization, we explored the polymerization of the targeted 2D-PPQVs (Scheme 1c). To this end, we employed C₃-symmetric HATN-6CHO (**3**) together with C₂-symmetric phosphonates **1** and **2** as monomers. Screening of the A₆B₂-type polycondensation was attempted under various solvothermal conditions in a temperature range of 120–150 °C. In detail, we screened the following bases: Rb₂CO₃, Cs₂CO₃, NaOH, and 1,8-diazabicyclo(5.4.0)undec-7-ene (DBU). In addition, we examined mixtures of *ortho*-dichlorobenzene (*o*-DCB), 1,4-dioxane, *N*-methyl-2-pyrrolidone (NMP), *N,N*-dimethylacetamide (DMAc), and mesitylene (Mes) as solvents for the polymerization. Polycondensation at 120 °C in a mixture of DMAc and Mes (1:1) in the presence of Cs₂CO₃ as the base was found to be the best condition for providing crystalline **2D-PPQV1** and **2D-PPQV2** (Scheme 1c). A summary of the synthesis conditions is presented in the Supporting Information (Table S1). After cooling the polymerization reaction to room temperature, the precipitate was filtered and washed with water, tetrahydrofuran (THF), NMP, *N,N*-dimethylformamide (DMF) and acetone several times. The resultant solid was dried under vacuum to afford **2D-PPQV1** and **2D-PPQV2** as red powders in yields of approximately 75 and 78%, respectively. To further prove the generality of this synthetic approach, the HWE polymerization of 5'-(4-formylphenyl)-[1,1':3',1''-terphenyl]-4,4''-dicarbaldehyde (**TFPB**) and 4,4'-bis(diethyl-phosphonomethyl)biphenyl (**2**) at 120 °C in DMAc + *o*-DCB (1:1) in the presence of Cs₂CO₃ as the base was also performed. The reaction scheme and analytical data for this achieved **2D-PPV1** are presented in the Supporting Information (Scheme S6 and Figure S34).

The chemical identity of **2D-PPQV1** and **2D-PPQV2** was confirmed by Fourier transform infrared (FTIR) spectroscopy (Figure 1a and Supporting Information) and ¹³C cross-polarization magic angle spinning (CP-MAS) NMR spectroscopy (Figure 1b and Supporting Information) in the solid-state. The FTIR spectra of **2D-PPQV1** and **2D-PPQV2** exhibit the same characteristic signals at 3025 cm⁻¹ (aromatic C–H valence vibrations, $\nu(\text{C–H})$) and at 1603 cm⁻¹ (vinylene stretches $\nu(\text{C=C})$). Weak carbonyl vibrations $\nu(\text{C=O})$ at approximately 1685 cm⁻¹ indicate the presence of -CHO end groups in the HATN moieties. In addition, weak signals at 950–1025 cm⁻¹ indicate the presence of phosphonate end groups (-CH₂PO(OEt)₂, $\nu(\text{P–O–C})$). Peaks attributed to tertiary benzene and quaternary benzene ring C atoms appear at chemical shifts of 130 and 140 ppm, respectively. Thermogravimetric analyses (TGAs) demonstrate that **2D-PPQV1** and **2D-PPQV2** both have high thermal stabilities up to 400 °C (Supporting Information, Figure S7). To demonstrate the excellent chemical stability against acidic and basic conditions, we immersed **2D-PPQV1** and **2D-PPQV2** in a potassium hydroxide solution (6 or 12 M KOH_{aq}) and hydrochloric acid (6 or 12 M HCl_{aq}), respectively, for five days. The PXRD and FTIR spectra did not identify any changes in the crystallinity or chemical nature of **2D-PPQV1** and **2D-PPQV2** (Supporting Information, Figures S4, and S5).



Scheme 1. Synthesis of 4,4'-di((E)-styryl)-1,1'-biphenyl (**4**), lin-PPV, **2D-PPQV1**, **2D-PPQV2**, **2D-CN-PPQV1**, and **2D-C=N-PPQV1**. Reaction conditions: (i) benzaldehyde (**5**), 4,4'-bis(diethyl-phosphonomethyl)biphenyl (**2**), Cs_2CO_3 , DMAC + Mes (1:1), 120 °C, 72 h, 80%; (ii) terephthalaldehyde (**6**), 4,4'-bis(diethyl-phosphonomethyl)biphenyl (**2**), Cs_2CO_3 , DMAC + Mes (1:1), 120 °C, 72 h, 79%; (iii) HATN-6CHO (**3**), 2,2'-(1,4-phenylene)diacetonitrile (**7**), DMAC + *o*-DCB (1:1), Cs_2CO_3 , 120 °C, 72 h, ca. 85%; (iv) HATN-6CHO (**3**), 1,4-bis(diethylphosphonomethyl)benzene (**1**) or 4,4'-bis(diethylphosphonomethyl)biphenyl (**2**), DMAC + Mes (1:1), Cs_2CO_3 , 120 °C, 72 h, ca. 78%; (v) HATN-6CHO (**3**), 1,4-diaminobenzene (**8**), DMAC + Mes (1:1), acetic acid, 120 °C, 72 h, ca. 73%.

The crystalline layered structures of **2D-PPQV1** and **2D-PPQV2** were manifested by experimental and simulated PXRD patterns (Figures 1c,d). The first reflection appeared at 3.6° for **2D-PPQV1** and 3.2° for **2D-PPQV2**, which are attributed to the (100) plane. In addition, **2D-PPQV2** showed a reflection at 5.6°, which is attributed to the (210) plane. The simulated PXRD patterns were optimized by using the density functional tight-binding (DFTB⁺) method.^[24] From the optimized monolayer structures, three stacking modes were investigated (Supporting Information), namely, eclipsed (AA), staggered (AB), and slipped AA (AA slip) stacking. These three stacking modes all yield lattice parameters that are too large with respect to the lattice parameters suggested by the PXRD pattern, and thus, a fourth stacking mode, wherein the linkers connect to centers in different “layers”, in effect creating a zig-zag layer, was modeled (AA mismatch). Both **2D-PPQV1** and **2D-PPQV2** adopted AA mismatch stacking, with per-layer stabilization energies of 159 and 180 kJ mol⁻¹, respectively (see a comparison in Table S2–S7, and Figure S15–S17). Pawley refinements were performed

using the Reflex package in Accelrys’s Materials Studio 7.0 software against the experimental pattern of **2D-PPQV1**, giving rise to the unit cell parameters of $a = 28.5 \text{ \AA}$, $b = 28.2 \text{ \AA}$, $c = 7.0 \text{ \AA}$, $\alpha = 90.8^\circ$, $\beta = 90.6^\circ$, and $\gamma = 57.1^\circ$, with agreement factors of $R_{\text{wp}} = 5.6\%$ and $R_{\text{p}} = 8.4\%$. Similarly, for **2D-PPQV2**, the resulting unit cell parameters were $a = 31.3 \text{ \AA}$, $b = 31.9 \text{ \AA}$, $c = 7.0 \text{ \AA}$, $\alpha = 89.9^\circ$, $\beta = 89.7^\circ$, and $\gamma = 60.0^\circ$, with agreement factors of $R_{\text{wp}} = 5.6\%$ and $R_{\text{p}} = 9.9\%$ (one unit cell contains two layers). The difference plots in Figures 1c and 1d show that the refined diffraction patterns are consistent with the experimental PXRD data.

The permanent porosity and pore size distribution of **2D-PPQV1** and **2D-PPQV2** were investigated by nitrogen physisorption analysis at 77 K. The Brunauer-Emmett-Teller (BET) surface areas of **2D-PPQV1** and **2D-PPQV2** were determined to be 440 m² g⁻¹ and 100 m² g⁻¹, respectively (Supporting Information, Figures S21, and S22). Further details of the BET measurements are described in the Supporting Information. The isotherm plots of both **2D-PPQV1** and **2D-PPQV2** displayed a rise in the low-pressure

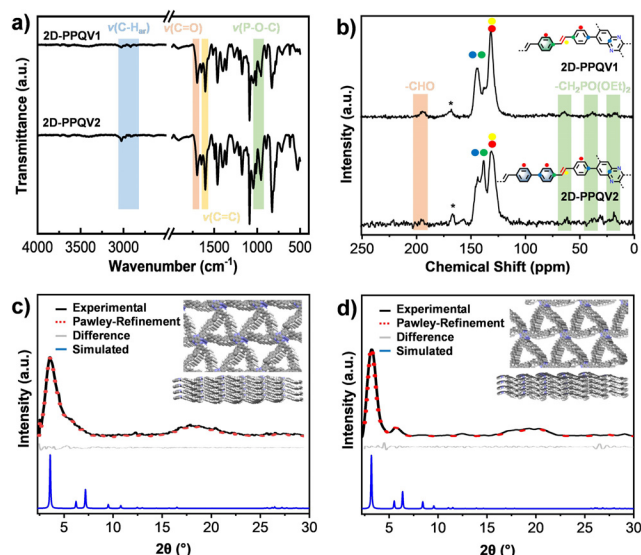


Figure 1. a) IR spectra and b) ^{13}C -ssNMR assignment of **2D-PPQV1** and **2D-PPQV2**, respectively, * residual dimethylformamide from the washing process; PXRD data of c) **2D-PPQV1** and d) **2D-PPQV2**: Experimental (black) and Pawley-refined PXRD (red), difference plot (gray), simulated PXRD with AA mismatch stacking (blue), and the model of the simulated eclipsed layer mismatch structure shown in the inset.

range ($P/P_0 = 0-0.1$), generating a typical type I nitrogen-sorption isotherm. Nonlocal density functional theory (NLDFE) was employed to calculate the pore size distributions, and the results show two main pore size distributions, approximately 7.7 Å and 13.8 Å for **2D-PPQV1** and 8.8 Å and 14.5 Å for **2D-PPQV2**, which are in good agreement with the theoretical values calculated from the eclipsed layer mismatch (AA mismatch) stacking model. Therefore, the above-described N_2 adsorption-desorption results, as well as the experimental and simulated PXRD patterns, clearly demonstrate the formation of the proclaimed dual-pore structure for **2D-PPQV1** and **2D-PPQV2**. Scanning electron microscopy (SEM) and high-resolution transmission electron microscopy (HR-TEM) of **2D-PPQV1** and **2D-PPQV2** disclose the layered morphologies after exfoliation by mechanical grinding and sonication in ethanol (Supporting Information, Figure S9).

Based on the above experimental results for the model compounds and 2D CPs, we propose the mechanism of the vinylene formation between diethyl [1,1'-biphenyl]-4-ylphosphonate (**I**) and [1,1'-biphenyl]-4-carbaldehyde (**III**) in four steps (Figure 2a). Moreover, we examined the energy profile of the HWE reaction in the gas phase by using density functional theory (DFT) calculations (Figure 2b). In the first step, the deprotonation of phosphonate species **I** under basic conditions (Cs_2CO_3) leads to carbanion species **II** ($E_{\text{II+III}} = +31.8 \text{ kJ mol}^{-1}$), which is resonance stabilized by the phosphonate group. Then, the reversible C–C bond formation is triggered by the nucleophilic attack of carbanion **II** at the carbonyl carbon of aldehyde **III** by bridging the carbonyl oxygen and phosphonate oxygen, forming a six-membered cyclic transition state with Cs^+ to give intermediate **IV** ($E =$

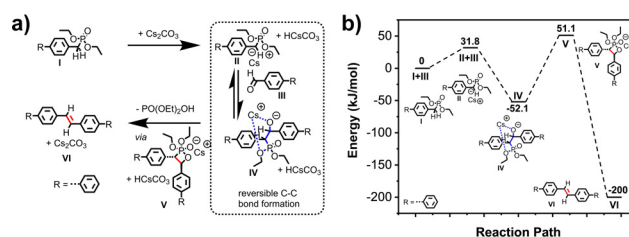


Figure 2. a) Proposed mechanism of the Horner–Wadsworth–Emmons reaction with Cs_2CO_3 as the base; b) energy profiles of the HWE reaction at different stages (I–VI), calculated in kJ mol^{-1} by using the DFT method.

$-52.1 \text{ kJ mol}^{-1}$). Afterward, oxaphosphetane **V** formation ($E = +51.1 \text{ kJ mol}^{-1}$) takes place. The subsequent irreversible elimination of $\text{PO}(\text{OEt})_2\text{OH}$ from oxaphosphetane **V** provides *trans*-vinylene **VI** ($E = -200 \text{ kJ mol}^{-1}$). Thus, the DFT calculations demonstrated the reversible C–C single bond formation during the HWE reaction, which is crucial for the achievement of crystalline 2D CPs.

Next, the optoelectronic properties of **2D-PPQV1** and **2D-PPQV2** were investigated by UV/Vis absorption and fluorescence spectroscopy in 2-propanol dispersions with a concentration of 0.2 mg mL^{-1} . To determine the critical role of the conjugation linkage on the optoelectronic properties of the corresponding 2D CPs, we also synthesized a cyano-vinylene-linked **2D-CN-PPQV1** via Knoevenagel polycondensation and an imine-linked COF **2D-C=N-PPQV1** (Scheme 1c and Supporting Information).^[15] Remarkably, UV/Vis absorption measurements reveal absorption edges at 575, 540, 598, and 592 nm, corresponding to optical energy gaps of 2.31, 2.39, 2.20, and 2.23 eV for **2D-C=N-PPQV1**, **2D-CN-PPQV1**, **2D-PPQV1**, and **2D-PPQV2**, respectively (Figure 3a and Tauc plot in the Supporting Information). The significantly lower optical energy gap for **2D-PPQV1** and **2D-PPQV2** in comparison to that of **2D-CN-PPQV1** reveals the superior conjugation of the unsubstituted vinylene-linked 2D CPs, which can be attributed to the structural planarity of their conjugated linkages and therefore increased electron delocalization over the whole sp^2 -carbon backbones.^[20]

The fluorescence spectra of **2D-C=N-PPQV1**, **2D-CN-PPQV1**, **2D-PPQV1**, and **2D-PPQV2** are presented in Figure 3b. Remarkably, all 2D CPs exhibited significantly different emission behavior. In comparison to the vinylene- and cyano-vinylene-linked 2D CPs, the imine-linked **2D-C=N-PPQV1** showed negligible fluorescence. Emission maxima were observed at 564, 629, and 629 nm for **2D-CN-PPQV1**, **2D-PPQV1**, and **2D-PPQV2**, respectively (Figure 3b,c). Therefore, the emission maxima of **2D-PPQV1** and **2D-PPQV2** underwent a large bathochromic shift of 65 nm compared to that of **2D-CN-PPQV1**, emphasizing the critical role of linkage for the enhanced conjugation of the whole 2D CP backbone. The photoluminescence quantum yield (PLQY) was measured to be 5.6, 2.5, and 2.7% for **2D-CN-PPQV1**, **2D-PPQV1**, and **2D-PPQV2**, respectively. We further performed UV/Vis absorption by acid-base titration, showing the reversible nature of the protonation of quinoxaline moieties. In contrast to those in 2-propanol, the absorption spectra of **2D-PPQV1** and **2D-PPQV2** in 6 M

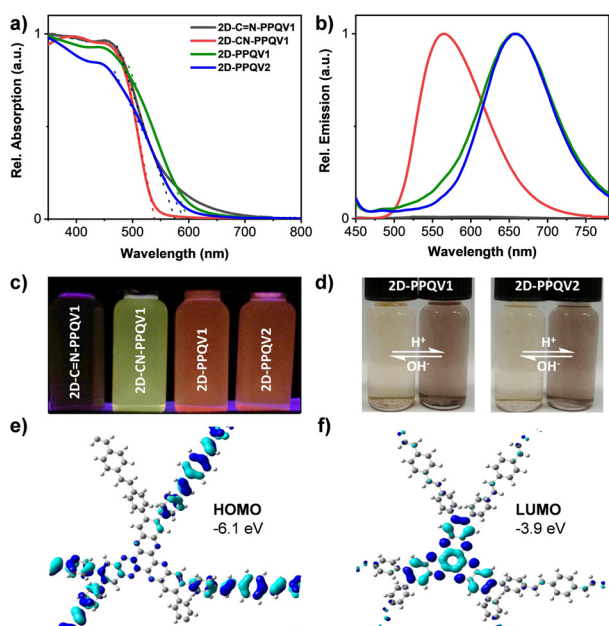


Figure 3. a) UV/Vis absorption and b) fluorescence ($\lambda_{ex} = 400$ nm) spectra of **2D-C=N-PPQV1** (black), **2D-CN-PPQV1** (red), **2D-PPQV1** (green), and **2D-PPQV2** (blue) (dispersions in 2-propanol, concentration = 0.2 mg mL⁻¹); c) photographs of the fluorescence emission ($\lambda_{ex} = 365$ nm) of **2D-C=N-PPQV1**, **2D-CN-PPQV1**, **2D-PPQV1**, and **2D-PPQV2**; d) photographs showing the reversible protonation of **2D-PPQV1** and **2D-PPQV2**; model of the e) HOMO topology and f) LUMO topology of **2D-PPQV1**, including the CV-observed energy levels of HOMO and LUMO.

HCl demonstrated a dramatic bathochromic shift, with an absorption edge in the near-infrared region at 850 nm. The shift of the absorption edges can be explained by the protonation of the quinoxaline moieties into cationic resonance structures, which are distributed over the HATN units. This great amount of resonance structures leads to a lack of charge separation.^[25] Thus, the optical energy gaps of the protonated **2D-PPQV1** and **2D-PPQV2** were determined to be 1.5 eV. Upon the addition of a 12 M NaOH solution to the HCl dispersion of **2D-PPQV1** and **2D-PPQV2**, the initial absorption spectra of the deprotonated 2D CPs were fully recovered (see Supporting Information Figure S30). The reversible protonation and deprotonation process of **2D-PPQV1** and **2D-PPQV2** was also visible by the color change of the dispersions (Figure 3d).

To determine the HOMO and LUMO levels of **2D-PPQV1** and **2D-PPQV2**, cyclic voltammetry measurements were performed in anhydrous acetonitrile (Supporting Information). **2D-PPQV1** and **2D-PPQV2** film electrodes show an anodic peak with an onset at 1.75 and 1.69 V, respectively. Based on this, the position of the HOMO was estimated to be -6.1 eV and -6.0 eV for **2D-PPQV1** and **2D-PPQV2**, respectively. A reduction behavior was not observed in the available potential window. The LUMO level of **2D-PPQV1** and **2D-PPQV2** was derived as -3.9 and -3.8 eV, respectively, based on the optical band gap and electrochemically determined HOMO level (see Supporting Information). The graphical representations of the HOMO and LUMO are

shown for **2D-PPQV1** in Figures 3e and 3f (and Supporting Information for **2D-PPQV2**). Clearly, the HOMO and LUMO are predominately separated. The HOMO is localized on the vinylene-phenylene linkage and partially on the HATN building block, whereas the LUMO is completely distributed on the HATN unit.

Finally, due to the robust fully conjugated structures, favorable energy gap, and energy level positions of the frontier orbital, **2D-PPQV2** was investigated as a proof-of-concept photocathode material for the photoelectrochemical hydrogen evolution reaction (PEC-HER). PEC-HER performance was evaluated in Ar-purged 0.1 M KOH using a Xe lamp (100 mW cm⁻², AM1.5 G) without further optimization. Under solar irradiation, **2D-PPQV2** exhibited a state-of-the-art photocurrent density of $\approx 8 \mu\text{A cm}^{-2}$ at 0 V vs. RHE for COF-type materials (Supporting Information, Figure S33a, Table S8). Electrochemical impedance spectroscopy (EIS) (Supporting Information, Figure S33b) confirmed that the charge-transfer resistance (R_{ct}) was reduced under light irradiation.

In summary, we present the first synthesis of unsubstituted vinylene-linked 2D-PPQVs via the HWE reaction of aryl phosphonate^[26] and aldehyde building blocks. The dual-pore structures of **2D-PPQV1** and **2D-PPQV2** were elucidated by PXRD, nitrogen physisorption measurements, and spectroscopic and microscopic characterizations. Density functional theory (DFT) simulations unveiled the crucial role of the initial reversible C-C single bond formation in the synthesis of crystalline 2D CPs. Importantly, optoelectronic property investigations demonstrated the superior conjugation of pristine vinylene-linked 2D CPs with narrow band gaps and large bathochromic shifts of emission compared to those synthesized by the Knoevenagel approach. Thus, HWE polymerization paves a new pathway to the development of unprecedented vinylene-linked 2D CPs with potential applications in (opto)electronics, sensing, catalysis, energy storage, and conversion.

Acknowledgements

This research was supported financially by the EU Graphene Flagship (GrapheneCore, No. 881603), the Collaborative Research Centre (CRC) 1415 “Chemistry of Synthetic Two-Dimensional Materials” (No. 417590517), H2020-MSCA-ITN (ULTIMATE, No. 813036), the Center for Advancing Electronics Dresden (cfaed), and the ERC Consolidator Grant (T2DCP, No. 819698). We thank M. Sc. SangWook Park for SEM, EDX, and TEM measurements, Dr. Philipp Schlender for PXRD measurements, Dr. Valeriya Tkachova for mass spectroscopy, Matthias Kluge for TGA measurements, M. Sc. Tobias Nickel for NMR measurements, M. Sc. Marcus Rauche for Raman measurements, Dr. Frank Simon, and M. Sc. Friedrich Schwotzer for the use of facilities. We also acknowledge Dipl.-Chem. Daniel Becker, Dr. Naisa Chandrasekhar, B. Sc. Albrecht Waentig, Dr. Thorsten Lohr, Dr. Renhao Dong, Dr. Irena Senkowska, and Dr. Hanjun Sun for helpful discussions, as well as B. Sc. Cindy Rau for practical support as a student research assistant. Computational

resources were provided by the Center for Information Services and High-Performance Computing (ZIH) of the Technische Universität Dresden. Open access funding enabled and organized by Projekt DEAL.

Conflict of interest

The authors declare no conflict of interest.

Keywords: 2D conjugated polymers · 2D covalent organic frameworks · 2D materials · Horner–Wadsworth–Emmons reaction · vinylene-linked

- [1] H. Shirakawa, E. J. Louis, A. G. MacDiarmid, C. K. Chiang, A. J. Heeger, *J. Chem. Soc. Chem. Commun.* **1977**, 578.
- [2] X. Zhao, X. Zhan, *Chem. Soc. Rev.* **2011**, *40*, 3728.
- [3] A. Moliton, R. C. Hiorns, *Polym. Int.* **2004**, *53*, 1397.
- [4] J. F. Mike, J. L. Lutkenhaus, *J. Polym. Sci. Part B* **2013**, *51*, 468.
- [5] S. Rochat, T. M. Swager, *ACS Appl. Mater. Interfaces* **2013**, *5*, 4488.
- [6] E. Smela, *Adv. Mater.* **2003**, *15*, 481.
- [7] M. D. McGehee, A. J. Heeger, *Adv. Mater.* **2000**, *12*, 1655.
- [8] J. Liu, R. Berger, K. Müllen, X. Feng in *From Polyphenylenes to Nanographenes and Graphene Nanoribbons* (Eds.: K. Müllen, X. Feng), Springer International Publishing, Cham, **2017**, pp. 1–32.
- [9] a) A. H. Castro Neto, F. Guinea, N. M. R. Peres, K. S. Novoselov, A. K. Geim, *Rev. Mod. Phys.* **2009**, *81*, 109; b) M. El Gemayel, A. Narita, L. F. Dössel, R. S. Sundaram, A. Kiersnowski, W. Pisula, M. R. Hansen, A. C. Ferrari, E. Orgiu, X. Feng, K. Müllen, P. Samorì, *Nanoscale* **2014**, *6*, 6301; c) X. Wang, Y. Ouyang, X. Li, H. Wang, J. Guo, H. Dai, *Physical Rev.* **2008**, *100*, 206803; d) K. A. Ritter, J. W. Lyding, *Nat. Mater.* **2009**, *8*, 235.
- [10] a) G. Galeotti, F. De Marchi, E. Hamzehpoor, O. MacLean, M. Rajeswara Rao, Y. Chen, L. V. Besteiro, D. Dettmann, L. Ferrari, F. Frezza, P. M. Sheverdyaeva, R. Liu, A. K. Kundu, P. Moras, M. Ebrahimi, M. C. Gallagher, F. Rosei, D. F. Perepichka, G. Contini, *Nat. Mater.* **2020**, *19*, 874; b) Y. Jing, T. Heine, *Nat. Mater.* **2020**, *19*, 823; c) H. Sahabudeen, H. Qi, B. A. Glatz, D. Tranca, R. Dong, Y. Hou, T. Zhang, C. Kuttner, T. Lehnert, G. Seifert, U. Kaiser, A. Fery, Z. Zheng, X. Feng, *Nat. Commun.* **2016**, *7*, 13461; d) R. Gutzler, D. F. Perepichka, *J. Am. Chem. Soc.* **2013**, *135*, 16585; e) M. Bieri, M. Treier, J. Cai, K. Ait-Mansour, P. Ruffieux, O. Gröning, P. Gröning, M. Kastler, R. Rieger, X. Feng, K. Müllen, R. Fasel, *Chem. Commun.* **2009**, 6919; f) R. H. Baughman, H. Eckhardt, M. Kertesz, *J. Chem. Phys.* **1987**, *87*, 6687; g) Tanaka, N. Kosai, H. Maruyama, H. Kobayashi, *Synth. Met.* **1998**, *92*, 253; h) N. Narita, S. Nagai, S. Suzuki, K. Nakao, *Phys. Rev. B* **1998**, *58*, 11009.
- [11] Y. Jin, Y. Hu, W. Zhang, *Nat. Rev. Chem.* **2017**, *1*, 0056.
- [12] A. Yassin, M. Trunk, F. Czerny, P. Fayon, A. Trewin, J. Schmidt, A. Thomas, *Adv. Funct. Mater.* **2017**, *27*, 1700233.
- [13] E. Jin, J. Li, K. Geng, Q. Jiang, H. Xu, Q. Xu, D. Jiang, *Nat. Commun.* **2018**, *9*, 4143.
- [14] Y. Zhao, H. Liu, C. Wu, Z. Zhang, Q. Pan, F. Hu, R. Wang, P. Li, X. Huang, Z. Li, *Angew. Chem. Int. Ed.* **2019**, *58*, 5376; *Angew. Chem.* **2019**, *131*, 5430.
- [15] S. Xu, G. Wang, B. P. Biswal, M. Addicoat, S. Paasch, W. Sheng, X. Zhuang, E. Brunner, T. Heine, R. Berger, X. Feng, *Angew. Chem. Int. Ed.* **2019**, *58*, 849; *Angew. Chem.* **2019**, *131*, 859.
- [16] a) X. Zhuang, W. Zhao, F. Zhang, Y. Cao, F. Liu, S. Bi, X. Feng, *Polym. Chem.* **2016**, *7*, 4176; b) E. Jin, M. Asada, Q. Xu, S. Dalapati, M. A. Addicoat, M. A. Brady, H. Xu, T. Nakamura, T. Heine, Q. Chen, D. Jiang, *Science* **2017**, *357*, 673; c) D. Becker, B. P. Biswal, P. Kaleńczuk, N. Chandrasekhar, L. Giebeler, M. Addicoat, S. Paasch, E. Brunner, K. Leo, A. Dianat, G. Cuniberti, R. Berger, X. Feng, *Chem. Eur. J.* **2019**, *25*, 6562; d) E. Jin, Z. Lan, Q. Jiang, K. Geng, G. Li, X. Wang, D. Jiang, *Chem* **2019**, *5*, 1632.
- [17] S. Bi, C. Yang, W. Zhang, J. Xu, L. Liu, D. Wu, X. Wang, Y. Han, Q. Liang, F. Zhang, *Nat. Commun.* **2019**, *10*, 2467.
- [18] J. Xu, Y. He, S. Bi, M. Wang, P. Yang, D. Wu, J. Wang, F. Zhang, *Angew. Chem. Int. Ed.* **2019**, *58*, 12065; *Angew. Chem.* **2019**, *131*, 12193.
- [19] T. Jadhav, Y. Fang, W. Patterson, C. Liu, E. Hamzehpoor, D. F. Perepichka, *Angew. Chem. Int. Ed.* **2019**, *58*, 13753; *Angew. Chem.* **2019**, *131*, 13891.
- [20] Y.-J. Cheng, S.-H. Yang, C.-S. Hsu, *Chem. Rev.* **2009**, *109*, 5868.
- [21] W. S. Wadsworth, *Org. React.* **1977**, *71*, 73.
- [22] K. Ando, *J. Org. Chem.* **1999**, *64*, 6815.
- [23] L. Kürti, B. Czákó, *Strategic applications of named reactions in organic synthesis. Background and detailed mechanisms; 250 named reactions*, Elsevier Acad. Press, Amsterdam, **2009**.
- [24] a) B. Aradi, B. Hourahine, T. Frauenheim, *J. Phys. Chem. A* **2007**, *111*, 5678; b) M. Elstner, D. Porezag, G. Jungnickel, J. Elsner, M. Haugk, T. Frauenheim, S. Suhai, G. Seifert, *Phys. Rev. B* **1998**, *58*, 7260.
- [25] E. Sawicki, B. Chastain, H. Bryant, A. Carr, *J. Org. Chem.* **1957**, *22*, 625.
- [26] H. Thomas, D. L. Pastoetter, M. Gmelch, T. Achenbach, A. Schlögl, M. Louis, X. Feng, S. Reineke, *Adv. Mater.* **2020**, *32*, 2000880.

Manuscript received: July 29, 2020

Revised manuscript received: September 9, 2020

Accepted manuscript online: September 22, 2020

Version of record online: October 22, 2020